Elastic and Inelastic Electron Scattering from Mn^{55}†

H. THEISSEN AND R. J. PETERSON
Electron Accelerator Laboratory, Yale University, New Haven, Connecticut 06520
AND
W. J. ALSTON, III
Boston University, Boston, Massachusetts 02215
AND
J. R. STEWART
New Haven College, New Haven, Connecticut
(Received 14 April 1969)

Elastic and inelastic electron scattering from Mn^{55} has been studied for incident electron energies between 25 and 60 MeV and scattering angles in the range 69°–149°. A partial-wave analysis of the elastic scattering data yielded a ground-state rms radius equal to 3.68±0.11 F, in good agreement with the muonic x-ray result. From inelastic scattering which covered excitation energies up to 3.5 MeV, reduced radiative-transition probabilities for excitations to levels at 0.98, 1.53, 1.88, 2.29, and 3.05 MeV have been deduced by a distorted-wave analysis. The transition probabilities are compared to those obtained from heavy-particle scattering and γ resonance fluorescence.

I. INTRODUCTION

INFORMATION about the nuclear structure of Mn^{55} has been obtained up to now mainly through reactions involving heavy particles. Some of the experiments have been used to extract transition strengths. The most recent results of this kind are available from inelastic α [1] and proton [2] scattering. These experiments show that the low-lying excited states of Mn^{55} exhibit some features of collectivity, although a description in terms of the weak-coupling model seems to be inadequate. In the weak-coupling model these states would be described as the coupling of a proton to the collective 2^+ state of a Cr^{54} core or a hole to the 2^+ state of Fe^{56}.

Another approach to studying Mn^{55} has been made with γ resonance fluorescence (RF).[3,4] From these measurements, ground-state radiation widths have been deduced. The results are in qualitative agreement with shell-model calculations.[5]

In order to obtain further insight into the nature of the low-lying states of Mn^{55}, we investigated the region up to excitation energies E_x=3.5 MeV by inelastic electron scattering. At higher excitation energies, the level density becomes too high to permit resolution of adjacent inelastic peaks. For this reason we could not investigate the octupole excitations to states above 4 MeV which have been observed in heavy-particle scattering.[1,6] Electron-scattering experiments are interesting in this case for the following reasons: The interaction of electrons with nuclei is purely electromagnetic, in contrast to heavy-particle scattering. This results in a more direct and straightforward determination of electromagnetic transition strengths. On the other hand, while γ RF determines the sum of the $M1$ and $E2$ partial widths, this electron scattering is almost exclusively sensitive to the $E2$ contribution. This is a result of the fact that for heavier nuclei, the electron scattering cross section[7] is dominated by the longitudinal term which is missing in the corresponding expression for γ excitation.

The inelastic cross sections were measured relative to the elastic ones. This required the knowledge of the elastic cross section, which in turn was determined by elastic scattering measurements relative to C^{12}. Although only a few points were taken, the rms radius of the ground-state charge distribution of Mn^{55} could be obtained.

II. EXPERIMENTAL METHOD

The experiment was carried out at the Yale 65-MeV electron accelerator. A description of the electron scattering equipment has been given previously.[8] No major changes have been introduced meanwhile. The beam was analyzed to about 0.25% of the incident energy and focused to a spot of approximately 2 mm in diam on the target. The beam-spot position, which was checked before and after a run by means of a ZnS screen, did not change by more than ±1 mm over peri-

† Research supported in part by the U.S. Atomic Energy Commission under Contract No. AT(30-1)2726.
[1] I. Gabrielli, B. G. Harvey, D. L. Hendrie, J. Mahoney, J. R. Meriwether, and T. Valentine, Nuovo Cimento (to be published).
[2] R. J. Peterson, Ann. Phys. (N.Y.) **53**, 40 (1969).
[3] E. C. Booth, B. Chasan, and K. A. Wright, Nucl. Phys. **57**, 403 (1964).
[4] W. J. Alston, III, H. H. Wilson, and E. C. Booth, Nucl. Phys. **A116**, 281 (1968).
[5] J. Vervier, Nucl. Phys. **78**, 497 (1966).
[6] R. J. Peterson, Phys. Letters **27B**, 446 (1968).
[7] T. deForest, Jr., and J. D. Walecka, Advan. Phys. **15**, 1 (1966).
[8] M. A. Duguay, C. K. Bockelman, T. H. Curtis, and R. A. Eisenstein, Phys. Rev. **163**, 1259 (1967).

TABLE I. Target data. ρx is the target thickness, $\bar{A}_r$ is the relative atomic weight.

Target	ρx (mg/cm²)	error (%)	$\bar{A}_r$
Mn^{55}	32.5	1.6	54.94
C^{12}	74.5	0.9	12.01

ods of 20 h. The energy stability was checked by taking an elastic peak at the beginning and at the end of a run. No shifts greater than 0.1% were observed. Of the six detectors lying in the focal plane of the spectrometer, three were used in this experiment. Dead-time losses were taken for only one of the channels. For the other channels the corrections were calculated under the assumption of a stable beam current. The dead-time losses never exceeded 1% of the counting rate. Typical average beam currents were 1–2 μA except at forward angles, where the dead-time losses necessitated smaller beam currents.

A 2×2 cm² metallic foil of natural manganese was used as a target. Because of the 100% natural abundance of Mn^{55}, no corrections for other isotopes were necessary. Data about admixtures of other elements than manganese could not be obtained from the manufacturer (Foote Mineral Co., Exton, Pa.). Major contaminations of heavier elements, which would make questionable particularly the elastic scattering results, were very unlikely because none of these were involved in the target electroplating. The carbon target was of natural isotopic composition, as was that used by Engfer and Türck in their measurement of the rms radius of carbon.[9] The thickness of the targets was measured by weighing and comparing the areas of enlarged shadow photographs of the targets with a square brass piece of 1×1 in.(±0.02%). By this method, the average thicknesses could be determined within an error of ±0.1%. An estimate of target nonuniformities was obtained by scanning the targets with a mechanical thickness gauge. The thickness variations were found to be about 1.6% for Mn^{55} and about 0.9% for C^{12}. The error of the target thicknesses was increased according to these uncertainties. The final result of the target thickness (ρx) measurements is entered in Table I. Also listed are the relative atomic weights ($\bar{A}_r$) used to calculate the ratio of the numbers of target atoms per cm². In order to average out part of the nonuniformities and to prevent overheating, the targets were rotated in the beam.

A special problem encountered with inelastic scattering was the instrumental scattering[8] caused by electromagnetic showers generated by electrons which hit the walls of the spectrometer vacuum chamber. Electrons scattered elastically by the target contribute most of this effect. These electrons produced a bump superimposed on the radiative tail, in our case in the region of about 2-MeV excitation energy. This bump had to be subtracted before analyzing the data. In order to do this an inelastic spectrum of C^{12} was taken up to about 3.5-MeV excitation energy. This part of the C^{12} spectrum is free of inelastic peaks, so that the difference between the calculated and measured tail could be used to determine the shape of the instrumental-scattering bump. Since there was no need for extreme accuracy, the Schiff approximation formula[10] was used to calculate the tail. The resulting curve was adjusted to the measured points well below the bump. The shape of the instrumental scattering bump obtained by this procedure was then fitted to those parts of the Mn^{55} spectrum which did not contain inelastic peaks, and subtracted. All this had to be done for each counter separately because of the different positions of the bump in each inelastic spectrum.

III. ELASTIC SCATTERING

Elastic data were taken at a constant scattering angle $\theta=129°$ for energies E_0 between 25 and 55 MeV. The target position remained unchanged during the whole

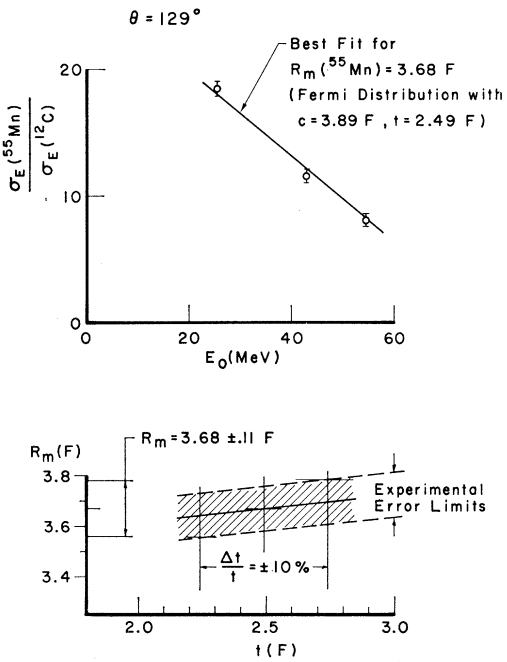

FIG. 1. Upper part: ratio of the differential elastic scattering cross section σ_E of Mn^{55} to that of C^{12} as a function of incident-electron energy E_0 at the scattering angle $\theta=129°$. The best theoretical fit is given by the solid line. Lower half: best-fit rms radius R_m of Mn^{55} as a function of the assumed skin thickness t (solid line). The dashed area indicates the acceptable range of R_m due to the experimental error.

[9] R. Engfer and D. Türck, Z. Physik **205**, 90 (1967).

[10] W. C. Barber, F. Berthold, G. Fricke, and F. E. Gudden, Phys. Rev. **120**, 2081 (1960).

TABLE II. Electron scattering data: E_0, electron energy; θ, scattering angle; q, momentum transfer; A, peak area; σ, differential scattering cross section. The subscripts E and I refer to elastic and inelastic, respectively; σ_{Mott}, Mott cross section.

Elastic scattering

E_0 (MeV)	θ (deg)	q_E (F^{-1})	$A_E(Mn^{55})/A_E(C^{12})$	Stat. error (%)	$\sigma_E(Mn^{55})/\sigma_E(C^{12})$	Total error (%)
25.68	129.0	0.236	1.76	0.6	18.5	2.3
42.75	129.0	0.393	1.11	0.4	11.7	2.2
54.41	129.0	0.500	0.78	0.3	8.14	2.1

Inelastic scattering

E_0 (MeV)	θ (deg)	q_I (F^{-1})	$A_I/A_E(10^{-4})$	$\sigma_E/\sigma_{\text{Mott}}$	$\sigma_I/\sigma_{\text{Mott}}(10^{-4})$	Stat. error (%)
			$E_x=0.98$ MeV, $\frac{9}{2}^-$			
60.25	69.1	0.348	0.7	0.613	0.4	92
60.23	89.0	0.428	6.4	0.427	2.7	9
60.22	109.0	0.496	11.8	0.290	3.4	10
60.13	129.0	0.548	25.3	0.203	5.1	7
60.14	149.0	0.584	36.1	0.153	5.5	9
51.19	149.0	0.497	12.4	0.289	3.6	11
54.43	129.0	0.496	9.1	0.290	2.7	12
			$E_x=1.88$ MeV, $\frac{7}{2}^-$			
60.25	69.1	0.345	0.5	0.613	0.3	148
60.23	89.0	0.425	2.5	0.427	1.1	30
60.22	109.0	0.492	5.4	0.290	1.6	18
60.13	129.0	0.544	8.2	0.203	1.7	15
60.14	149.0	0.580	6.1	0.153	0.9	86
51.19	149.0	0.492	8.2	0.289	2.4	14
54.43	129.0	0.492	6.5	0.290	1.9	13
			$E_x=2.29$ MeV			
60.25	69.1	0.344	3.0	0.613	1.8	8
60.23	89.0	0.424	9.4	0.427	4.0	7
60.22	109.0	0.491	8.8	0.290	2.6	26
60.13	129.0	0.542	17.9	0.203	3.6	10
60.14	149.0	0.578	28.3	0.153	4.3	22
51.19	149.0	0.490	14.0	0.289	4.0	10
54.43	129.0	0.490	10.9	0.290	3.2	8

run. This reduced the possibility of systematic errors in the effective target thicknesses and solid angles. The elastic peaks were integrated separately for each counter, the low-energy cutoff being set at least 0.7 MeV below the position of the peak maximum. Since the first excited level of Mn^{55} at 126 keV could not be resolved from the elastic peak, its contribution to the elastic-peak area had to be subtracted. A distorted-wave calculation showed that the $E2$ and $M1$ contributions of the 126-keV transition to the elastic-peak area, even at the highest momentum transfer ($q=0.45$ F^{-1}, $E_0=54.4$ MeV, $\theta=129°$), were less than 3×10^{-3} and 10^{-5}, respectively. These numbers were obtained from the most recent values for the reduced transition probabilities $B(E2\uparrow)=311$ F^4 [11] and $B(M1\uparrow)=1.2\times10^{-3}$ F^2.[12] Compared to the statistical error, the $M1$ contribution was negligibly small; hence only the electric excitation was taken into account. The peak areas had also to be corrected for the scattering from the magnetic dipole and electric quadrupole moment of the ground state. These corrections were estimated in a plane-wave Born approximation. For a magnetic moment[13] $\mu=3.5$ μ_N and a quadrupole moment[13] $Q=0.4\times10^{-24}$ cm^2, the contributions to the elastic-peak area turned out to be together less than 0.3%. The remaining corrections included the usual Schwinger,[14] bremsstrahlung,[15] and Landau[16] corrections. In order to simplify the further analysis, the Mn^{55} and C^{12} peak areas were normalized to a common average energy at

[11] R. C. Ritter, P. H. Stelson, F. K. McGowan, and R. L. Robinson, Phys. Rev. **128**, 2320(1962).

[12] R. E. Holland and F. J. Lynch, Phys. Rev. **121**, 1464 (1961).

[13] *Nuclear Moments*, Appendix 1 to *Nuclear Data Sheets*, compiled by G. H. Fuller and V. W. Cohen (U.S. Government Printing Office, Washington, D.C., 1965).

[14] J. W. Motz, H. Olsen, and H. W. Koch, Rev. Mod. Phys. **36**, 881 (1964).

[15] H. Crannell, Phys. Rev. **148**, 1107 (1966).

[16] L. Landau, J. Phys. (USSR) **8**, 201 (1944).

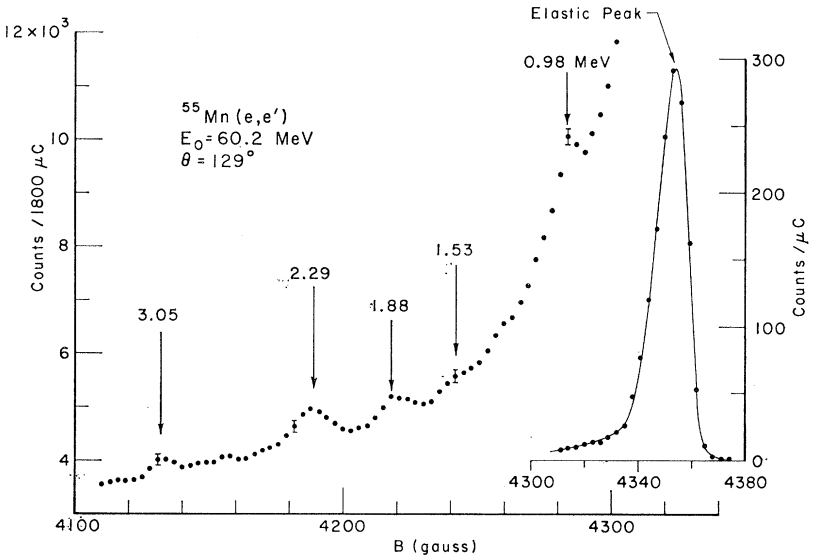

FIG. 2. Spectrum of electrons scattered from Mn^{55} at an incident-electron energy $E_0=60.2$ MeV and a scattering angle of $\theta=129°$. The instrumental scattering has been subtracted.

each point. Small energy shifts between the Mn^{55} and C^{12} peaks were due to different nuclear recoil and different ionization losses. The normalization was done by multiplying the areas by the ratio of the average-energy cross section to actual-energy cross section. These cross sections were calculated by partial-wave analysis using the results of Quitmann *et al.*[17] and Bentz[18] for the rms radii of Mn^{55} and C^{12}. In all cases, the normalization factors deviated from unity by less than 0.4%. The averages of the areas $A(Mn^{55})$ and $A(C^{12})$ over the three counters and the ratios $A(Mn^{55})/A(C^{12})$ are entered in Table II, column 4. Division by $(\rho x/\bar{A}_r)$-$Mn^{55}/(\rho x/\bar{A}_r)C^{12}=0.0951\pm0.0024$ yielded the cross section ratios $\sigma_E(Mn^{55})/\sigma_E(C^{12})$ listed in column 6 of Table II.

The rms radius of Mn^{55} was obtained by fitting the experimental points to curves derived from calculations done with a partial-wave code written by Rawitscher and Fischer.[19] The C^{12} charge distribution was taken to be of the shell-model type with $a=1.648$ F and $\alpha=1.056$[18] ($R_m(C^{12})=2.395$ F). For Mn^{55}, a Fermi-type charge distribution with a 90%–10% skin thickness of $t=2.49$ F was assumed, the half-radius c being the fitting parameter. The best fit was obtained for $c=3.89$ F, giving an rms radius $R_m(Mn^{55})=3.68$ F. The upper part of Fig. 1 shows the corresponding curve for the cross-section ratios $\sigma_E(Mn^{55})/\sigma_E(F^{12})$ versus energy E_0. From the goodness of fit,[20] a statistical error of ±0.04 F was deduced, and fits to the cross-section ratios shifted up and down by the systematic error of the target thicknesses (Table I) resulted in a final systematic error in the rms radius of ±0.05 F. In order to check the parameter dependence of the rms radius, the data were further analyzed for a certain range of Fermi-distribution parameters. The result is shown in the lower part of Fig. 1. If one allows the skin thickness to assume values between $\pm10\%$ of the original value $t=2.49$ F, the rms radius change is ±0.02 F. This demonstrates the weak-model dependence previously noted for low-energy electron scattering.[21,22] The final result, including all errors and parameter dependence, is therefore $R_m(Mn^{55})=3.68\pm0.11$ F. From this, one obtains for the quantity $r_0=(5/3)^{1/2}R_m/A^{1/3}$, disregarding the error due to parameter dependence, $r_0=1.25\pm0.03$ F.

This result is in very good agreement with the muonic x-ray value of $r_0=1.263\pm0.023$ F reported by Quitmann *et al.*[17] The fact that the latter was obtained for a family-II type of charge distribution should not invalidate this conclusion, because there is but little difference between a family-II and a Fermi distribution for a fixed rms radius.[22]

IV. INELASTIC SCATTERING

Inelastic spectra were measured for five angles (69°, 89°, 109°, 129°, and 149°) at an energy of $E_0=60.2$ MeV. Because of the nonzero ground-state spin of Mn^{55}, mixed transitions, e.g., $E2$-$M1$ mixtures, were possible. In order to determine the magnetic contributions or at least give an upper limit for them, additional data were taken at $E_0=54.4$ MeV, $\theta=129°$, and $E_0=$

[17] D. Quitmann, R. Engfer, U. Hegel, P. Brix, G. Backenstoss, K. Goebel, and B. Stadler, Nucl. Phys. **51**, 609 (1964).
[18] H. Bentz, Z. Physik (to be published).
[19] G. H. Rawitscher, Phys. Rev. **112**, 1274 (1958); G. H. Rawitscher and C. R. Fischer, *ibid.* **122**, 1330 (1961).
[20] R. A. Eisenstein, D. W. Madsen, H. Theissen, L. S. Cardman, and C. K. Bockelman (unpublished).
[21] L. R. B. Elton, *Nuclear Sizes* (Oxford University Press, London, 1961).
[22] R. Engfer, Z. Physik **192**, 29 (1966).

51.2 MeV, $\theta=149°$. Together with the point at $E_0=60.2$ MeV, $\theta=109°$, they form a set of measurements at constant inelastic momentum transfer $q_I=0.49$ F^{-1}. Calculations in plane-wave Born approximation show that in this case the inelastic form factor plotted against the quantity $\frac{1}{2}(1+2\tan^2\frac{1}{2}\theta)$[23] is a horizontal straight line if there are only longitudinal contributions. Any nonzero slope, on the other hand, indicates transverse admixtures. In cases where the transverse-electric term can be neglected, the slope directly gives the magnetic form factor. The same general behavior as that predicted by the plane-wave Born approximation also holds true for the quantity $\sigma_I/\sigma_{\text{Mott}}$, i.e., the differential inelastic cross section divided by the Mott cross section obtained from a distorted-wave analysis. Calculations for an assumed $E2$-$M1$ transition in Mn^{55} ($E_x=2.3$ MeV, $q_I=0.34$ F^{-1}) employing the DUELS distorted-wave Born-approximation code[24] confirmed this. Although certain (simple) assumptions had to be made about the transition charge current, and magnetization densities, which will be given later, the result should be fairly model-independent because of the low momentum transfer. In our special example, the deviations from a straight line were less than 2.5% for the angular range between 109° and 149°.

The data reduction started with the subtraction of the instrumental scattering as described in Sec. II. After that, the spectra of the three counters were combined by shifting them according to their elastic-peak positions and adding up all counts falling into corresponding energy intervals. Figure 2 shows an example of the resulting spectrum. Three prominent peaks at excitation energies $E_x=0.98$, 1.88, and 2.29 MeV, and two less distinct bumps at $E_x=1.53$ and 3.05 MeV can be seen. All excitation energies could be determined within an error of ±0.03 MeV. Hence the first three peaks could clearly be identified as the excitation of the 983-, 1527-, and 1884-keV levels of Mn^{55}.[25] In the case of the peak at 2.29-MeV excitation energy, a slight broadening could not be ruled out. It might therefore correspond to an excitation of two nearby levels at 2.25 MeV and 2.37 keV which are observed in α-particle[1] and proton[2] scattering. The same experiments showed, among other states, a level at 3.05-MeV excitation energy. Because of the high level density in this region, however, it is questionable whether this is the same transition as the one observed in this experiment.

The ratios of the inelastic to elastic peak areas were determined by a least-squares fitting routine that adjusted the observed elastic peak in position and height to the inelastic ones. This is justified, provided that both peaks have the same shape. Detailed investigations[26] have shown that this is true except for insignificant differences in the radiative tails.[27] The spectrum was fitted step-by-step starting with the peak at the lowest excitation energy. The resulting ratios A_I/A_E of the inelastic to elastic peak areas were multiplied by the elastic cross section to give the inelastic cross section σ_I. The elastic cross section was calculated from the previously determined ground-state charge-distribution parameters. Table II shows the numerical values of A_I/A_E and the cross sections divided by the Mott cross section σ_{Mott} for the three strongest transitions.

The reduced transition probabilities were obtained by normalizing the calculated curves to the observed points. The calculations were done in distorted-partial-wave analysis using the code DUELS.[24] This program generated the inelastic cross section for a reduced transition probability of $1\,\text{F}^{2L}$, L being the multipolarity of the transition. The transition charge density was taken to be that of an incompressible and irrotational liquid drop[28] with the same values for the half-radius c and the skin thickness t as the ground-state distribution, resulting in a transition radius of $R_{\text{tr}}=5.24$ F. The actual form of the transition charge density is then, apart from a normalization factor, the derivative of the ground-state distribution. The transition current density is obtained by solving the continuity equation for the above transition charge density. For the transition density of the magnetization, the same functional dependence as that of the transition charge density was assumed. This is, of course, a very crude approximation because the magnetization is related to the nuclear matter rather than the charge distribution, and both distributions are not necessarily identical. But it should not completely invalidate the results inasmuch as it turned out that the magnetic contributions were so small that only upper limits could be given for them.

All angular distributions could be fitted under the assumption of an electric quadrupole transition. This is shown in Fig. 3 for the 0.98-, 1.88-, and 2.29-MeV transitions. The resulting $B(E2\uparrow)$ values are given in Table III, row 1. The fits for the 1.53- and 3.05-MeV excitations gave less accurate results because of the large error bars associated with the data points. Their $B(E2\uparrow)$ values in Table III are therefore placed in parentheses, being valid only under the assumption of a pure $E2$ transition. In the case of the level at $E_x=3.05$ MeV, an $L=3$ excitation could not be excluded. An analysis based on this assumption, however, gave the very large transition strength of $B(E3\uparrow)=5600\pm1600$ F^6. No such strong octupole excitation near 3.0 MeV is seen in heavy-particle inelastic scattering,[1,2]

[23] Neglecting terms of the order of $(E_x/E_0)^2$.
[24] S. T. Tuan and L. E. Wright, Nucl. Instr. Methods **60**, 70 (1968).
[25] H. Mazari, A. Sperduto, and W. W. Buechner, Phys. Rev. **108**, 103 (1957).
[26] O. Titze, Laborbericht No. 31, Institut f. Technische Kernphysic, Technische Hochschule Darmstadt, Germany (unpublished).
[27] T. Perez y Zorba, J. Phys. Radium **22**, 733 (1961).
[28] L. I. Tassie, Australian J. Phys. **9**, 407 (1956).

TABLE III. Results for inelastic scattering. E_x is the excitation energy, J^π is the spin and parity of corresponding level, $B(E2\uparrow)$ is the reduced transition probability, and Γ_γ^0 is the ground-state radiation width. The $B(E2)$'s quoted as the results of this work have been obtained assuming the strict hydrodynamical model. The model dependence was taken into account by adding a ±15% uncertainty to the statistical error (see text).

	E_x(MeV), J^π 0.98 ($\frac{9}{2}^-$)	1.53 ($\frac{3}{2}^-$)	1.88 ($\frac{7}{2}^-$)	(2.29)	(3.05)
$B(E2\uparrow)$ (F^4), this work	147±30	(28±16)	68±15	154±30	(34±10)
$B(E2\uparrow)$ (F^4), (α,α')[a]	167.0	...	119.0	89.4[d]	
$B(E2\uparrow)$ (F^4), (p,p')[b]	201	...	125	125[d]	
$\Gamma_\gamma^0(E2)$ (10^{-3} eV), this work	0.066±0.014	(0.28±0.16)	0.96±0.21	...	...
$\Gamma_\gamma^0(M1+E2)$ (10^{-3} eV), (RF)[c]	...	8±3	41±6	...	...
$\delta^2=\Gamma_\gamma^0(E2)/\Gamma_\gamma^0(M1)$	...	(0.04±0.04)	0.024±0.009	...	...

[a] Reference 1.
[b] Reference 2.
[c] Reference 4.
[d] Strengths of the 2.25- and 2.37-MeV transitions were added.

and we reject the possibility of our data being $L=3$ in nature.

The model dependence of the transition probabilities is hard to estimate. Duguay *et al.*[8] investigated the effect of varying the parameters of the transition charge density (Figs. 27 and 28 of that work). For an $E2$ transition in Ni^{58} and electron energies around 60 MeV, this parameter dependence leads to uncertainties of approximately ±15% in the transition probability as well as in the transition radius. It is generally believed that this is also a fairly good estimate of the model dependence. Because of the similar sizes of Mn^{55} and Ni^{58} and the nearly equal energies used in both experiments, we adopted the above result for the uncertainty due to parameter variation and algebraically added ±15% to the statistical error of the $B(E2)$'s. This produced the over-all uncertainties listed in Table III.

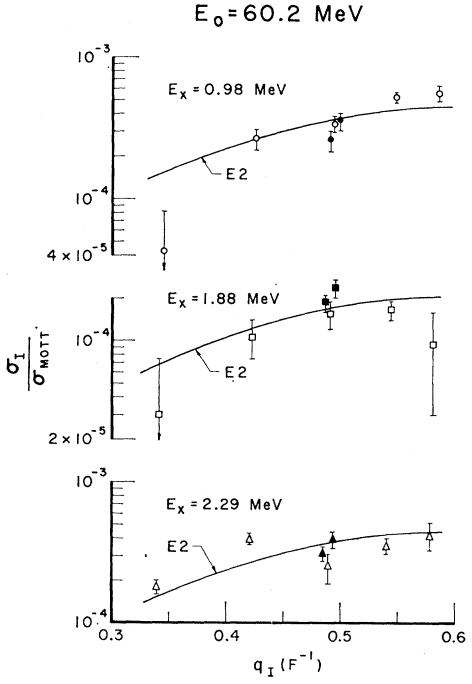

FIG. 3. Differential inelastic cross section σ_I in units of the Mott cross section σ_{Mott} as a function of the inelastic momentum transfer q_I for the 0.98-, 1.88-, and 2.29-MeV transitions in Mn^{55}. Open symbols represent points taken at $E_0=60.2$ MeV. Closed symbols refer to additional points taken at $q_I=0.49$ F^{-1}, but different electron energies (see text). The best theoretical fits assuming pure $E2$ transitions are given by the solid lines.

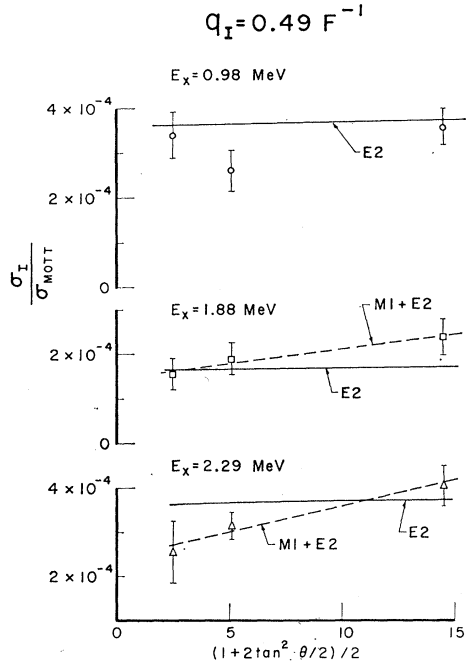

FIG. 4. Differential inelastic cross section σ_I divided by the Mott cross section σ_{Mott}, taken at constant inelastic momentum transfer, as a function of $\frac{1}{2}(1+2\tan^2\frac{1}{2}\theta)$, i.e., points at $q_I=0.49$ F^{-1} of Fig. 3 replotted. The solid lines represent the best theoretical fits from Fig. 3 for pure $E2$ transitions. The dashed lines are obtained under the assumption of an $E2$-$M1$ mixture (see text).

Magnetic contributions, as mentioned before, can be determined by constant momentum-transfer measurements. In Fig. 4, the three points of Fig. 3 at $q=0.49$ F^{-1} were therefore replotted against the quantity $\frac{1}{2}(1+2\tan^2\theta)$. Again only the data for the three most prominent peaks are shown. The solid lines in Fig. 4 represent the best-fit curves obtained previously under the assumption of a pure $E2$ transition. In all cases, since there are no significant deviations from these nearly horizontal lines, the magnetic contributions to the cross sections must be small. On the other hand, a nonzero slope could not be excluded for the 1.88- and 2.29-MeV transitions. If one tentatively assumes $M1$ admixtures (higher multipolarities can be neglected because their relative contributions are decreasing with q^{2L-2}) and fits the constant-q data only, then the dashed lines are obtained. The resulting transition probabilities included the zero and could therefore be considered only as upper limits. The analysis yielded $B(M1\uparrow)<0.03$ F^2 for the 1.88-MeV transition and $B(M1\uparrow)<0.04$ F^2 for the 2.29-MeV transition.

Comparison of our results for the reduced transition probabilities with those obtained from inelastic α scattering[1] (row 2 of Table III) shows fairly good agreement for the 0.98-MeV level. In the case of the 1.88-MeV state, however, α scattering gives a $B(E2)$ differing from our result by almost a factor of 2. The peak at 2.29 MeV, as mentioned before, does not have its counterpart in the α spectrum. A comparison is therefore questionable. Summing the strengths of the two nearby levels at 2.25 and 2.37 MeV observed in α scattering leads to a smaller $B(E2)$ than our value. Converting the βR values of the proton-scattering work[2] into transition probabilities (row 3 of Table III) gives qualitatively the same picture. The discrepancies between proton and electron scattering, however, are somewhat larger than in the former case.

Attempts to remove these discrepancies have been made by introducing different "interaction radii"[29] for the three reactions. However, this leads to even bigger $B(E2)$'s for the heavy-particle scattering, the enhancement being the square of the ratio of the heavy-particle interaction radius to that of the electron. Thus the discrepancy is even worse in this case, except for the 2.29-MeV transition, where a comparison is questionable. Since the interpretation of heavy-particle scattering experiments in terms of electromagnetic transition strengths involves more model assumptions than the analysis of electron scattering data, we believe that the results presented here are the more reliable ones for the $B(E2)$ values.

A comparison between RF[3,4] and electron scattering results, as far as results are available for both experiments, shows that the $E2$ admixtures in the combined $M1+E2$ widths comprise only a few percent. The widths obtained from these experiments (row 5 of Table II) are therefore almost pure $M1$ in character. Combing the results of both measurements leads to the mixing ratios shown in the last row of Table III. It should be emphasized again that RF and electron scattering are generally not equal in their sensitivities to electric and magnetic transitions, although the basic interaction is purely electromagnetic in both cases. The above discussed transitions are a good example for this: Although in terms of ground-state radiation widths which are measured at these low excitations by RF, the $E2$ part is small compared to the $M1$ part, it is only this quantity which can be obtained with a reasonable accuracy from electron scattering.

On the other hand, we want to mention that this experiment was only a first attempt to analyze mixed transitions in medium-heavy nuclei. With improvements in statistics it should be possible to determine the magnetic as well as the electric transition probability and thus mixing ratios for these nuclei from electron scattering alone.

ACKNOWLEDGMENTS

We are greatly indebted to Professor C. K. Bockelman for his advice and continuous interest in our experiment. Special thanks go to Professor H. L. Schultz, in whose laboratory the experiments were performed. For operating the accelerator and the maintanance of the experimental equipment we wish to thank the accelerator laboratory staff. The help received from other members of the Yale electron scattering group in taking and analyzing data is also acknowledged. Two of us (W. J. A. and J. R. S.) want to express gratitude for the kind hospitality extended to them during their stay at Yale. In addition, the Graduate School of Boston University is thanked for its financial support of one of the authors (W. J. A.).

[29] E. P. Lippincott and A. M. Bernstein, Phys. Rev. **163**, 1170 (1967).